Analysis of gold in rock samples using laser-induced breakdown spectroscopy: matrix and heterogeneity effects

Rifai, Kheireddine; Laflamme, Marcel; Constantin, Marc; Vidal, François; Sabsabi, Mohamad; Blouin, Alain; Bouchard, Paul; Fytas, Konstantinos; Castello, Maryline; Kamwa, Blandine Nguegang

Publisher's version / Version de l'éditeur:
https://doi.org/10.1016/j.sab.2017.06.004
Spectrochimica Acta Part B: Atomic Spectroscopy, 134, pp. 33-41, 2017-06-06

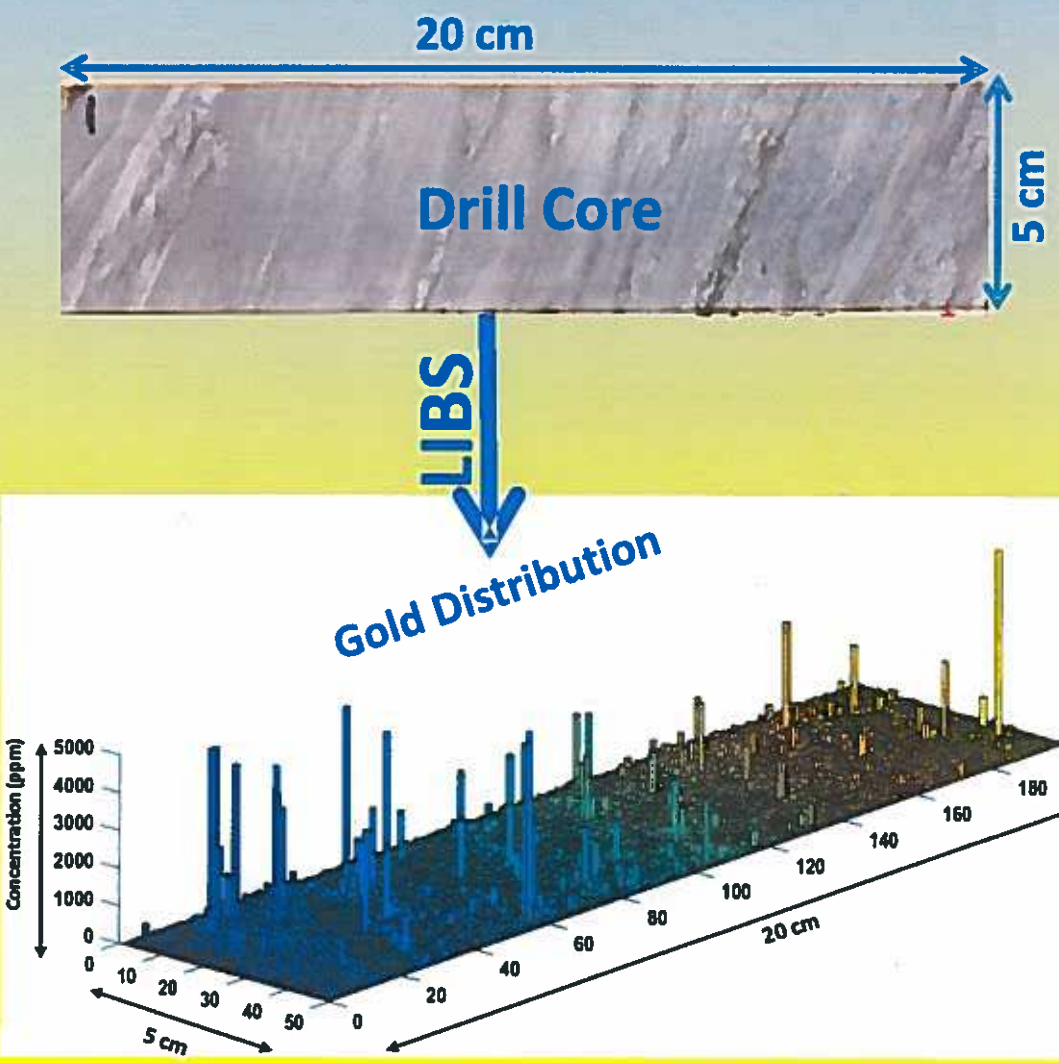
20 cm
Drill Core
5 cm
LIBS
Gold Distribution
Concentration (ppm)
5000
4000
3000
2000
1000
0
0
10
20
30
40
50
5 cm
0
20
40
60
80
100
120
140
160
180
200
20 cm

- First use of LIBS for quantitative analysis of gold in ore samples
- Development of chemometric approaches coupled to adequate internal reference for normalisation based on line intensity ratio to continuum to minimise matrix effect for gold determination
- Possibility of using LIBS for gold detection in the ppm range
- Showing LIBS as a useful tool for gold detection and the challenges to be resolved to improve its analytical performances
- Spectroscopy of gold in ore samples.

Analysis of gold in rock samples using laser-induced breakdown spectroscopy: matrix and heterogeneity effects

Kheireddine Rifai[1,2,*]	KheirEddine.Rifai@cnrc-nrc.gc.ca
Marcel Laflamme[1]	marcel.laflamme@gmn.ulaval.ca
Marc Constantin[1]	Marc.Constantin@ggl.ulaval.ca
François Vidal[3]	Vidal@emt.inrs.ca
Mohamad Sabsabi[2]	Mohamad.Sabsabi@cnrc-nrc.gc.ca
Blouin, Alain[2]	Alain.Blouin@cnrc-nrc.gc.ca
Bouchard, Paul[2]	Paul.Bouchard@cnrc-nrc.gc.ca
Konstantinos Fytas[1]	Kostas.Fytas@gmn.ulaval.ca
Maryline Castello[1]	maryline.castello.1@ulaval.ca
Blandine Nguegang Kamwa[1]	blandine.nguegang-kamwa.1@ulaval.ca

[1]Université Laval, Faculté des sciences et de génie, 1045 Avenue de la Médecine, Québec, QC G1V 0A6

[2]National Research Council of Canada, 75 de Mortagne Blvd., Boucherville, Québec, Canada J4B 6Y4.

[3]INRS-Énergie, Matériaux et Télécommunications, 1650 Boul. Lionel Boulet, Varennes, Québec, Canada J3X 1S2.

[*] Author to whom correspondence should be sent

Kheireddine Rifai Tel: 450-641-5849 Fax: 450-641-5106

Abstract

We used the laser-induced breakdown spectroscopy (LIBS) technique to determine the concentration of gold in rock samples. 44 reference materials (mostly compressed fine powders) of various chemical compositions, with a quasi-homogeneous concentration of gold varying from 0 to 1000 ppm, were used to establish the calibration curve for the Au I 267.59 nm line. A chemometric study based on the principal component analysis (PCA) showed that ~83% of the LIBS spectra variations are attributable to the presence of iron in the samples. Two distinct branches were obtained in the calibration curve: one for Si-rich samples (< 5% of iron) and one for Fe-rich samples (> 13% of iron) with limits of detection of 0.8 ppm and 1.5 ppm, respectively. Different normalization schemes of the gold signal were tested in order to reduce the matrix effects. The LIBS analysis was performed on various mineral samples of practical interest and compared to the reference values, namely two Si-rich uncompressed ore powders, fine and granular, and three bulk drill cores. It was found that the agreement between the reference and LIBS-determined gold concentrations is best for homogenized fine powders. For the granular powder and drill cores the LIBS values were higher (46-82%) and lower (~50%), respectively, than the reference values.

1. Introduction

Gold mines are very important economic assets for many countries in the world, which translate into billions of dollars annually in production and in thousands of direct jobs. However, mining industries are facing increasing decisional challenges associated with lower grade ore and complexity of mineralization with higher impurity levels [1] which imply more frequent sample analyses in the production process. Furthermore, mining sample analyses performed using conventional techniques based on wet chemistry or fire assay involve wait times of at least 24 hours, causing production delays on the mining or exploration sites and thus increasing the operating and production costs.

In order to address these issues, mining industry is on the lookout for new technologies that meet their cost reduction need. One of these innovative technologies, whose development would be a major breakthrough, is the measure of precious metal concentration in real time and on site during the different exploration and mining production stages. [2] In the case of gold, this technology should be able to measure an average concentration down to ~1 ppm since gold is still worth extracting for such low a concentration.

Existing technology for the direct analysis of solid sample, such as infrared spectroscopy, allows determining the mineralogy of the rock samples (quartz, pyrite, chalcopyrite, sphalerite, arsenopyrite, etc.), but the elemental composition is out of reach with this technique. [3] Furthermore, x-ray fluorescence has been used successfully for determining the concentration of some basic metals such as copper, zinc and nickel; it is however inadequate for quantifying gold concentration, because of low sensitivity and poor limits of detection. [4] In

addition, those based on portable X Ray fluorescence (XRF) are not sensitive enough for gold detection in the ppm range required by the industry and suffers from interference with zinc and iron lines which gives false values for gold and compromises its determination. Laser-induced breakdown spectroscopy (LIBS) appears to be a potential technique for performing elemental analyses under the desired real time and on site conditions. LIBS is an optical diagnostic technique based on emission spectroscopy. It uses a laser beam of moderate power focused onto a material sample (solid, liquid or gas) to atomize the surface and generate luminous plasma. The light emitted by the plasma is then spectrally analyzed to determine the chemical composition of the sample. By using calibrated samples, it is then possible to determine accurately the concentration of the elements contained in any sample of the same family of composition. [5] The main potential advantages of LIBS for the mining industry over conventional analytical techniques would be its ability to analyze samples on site and remotely, with minimal or no sample preparation at all regardless the nature of the sample [5].

LIBS has already been considered for the analysis of ore samples. Most of these investigations were dedicated to the identification of mineral groups, with a few to the quantitative or semi-quantitative analysis of the minor and major elements contained in ore samples. Among the studies performed, a large part dealt with iron ores, as for instance: the qualitative and semi quantitative multi-element analysis of iron ore [6, 7], the quantitative analysis of manganese and silicon in powdered iron ore samples [8], the potential effect of particle size and ore mineralogy in iron ore samples [9, 10], the semi quantitative analysis performed on

bore drill cores [11], and the quantitative multi-element analysis of iron ore pellets [12]. More recently, Dalm and Boxten seeked to distinguish between the economic and sub-economic value of gold in epithermal Au-Ag deposits [13]. They reported that a relationship may exist between the alteration mineralogy of samples and their Au content. For instance, the Na / Al peak intensity ratio from LIBS spectra could be used to predict the Au grade of the samples.

To the best of our knowledge, there is no study devoted to the LIBS analysis of gold in ore samples. This is likely due to four main challenges related to such an investigation: (1) heterogeneity of the gold distribution and the lack of natural gold ore reference samples, (2) variation of the mineralogical matrix in ore samples, (3) complexity of their natural mixing matrices for analytical purposes, and (4) the complexity of characterisation of the laser induced plasmas. In terms of a functional LIBS-based device, these challenges translate into: (1) sampling appropriately the surface of the mineral in order to evaluate accurately the gold concentration, (2) resolving the matrix effects which result in variations of the gold spectroscopic signal with the compositions of the ore, (3) finding ways for preparing synthetic samples to match natural rock samples for quantitative analysis, and (4) conciliating bulk analysis by conventional techniques based on wet chemistry versus surface analysis given by LIBS.

In this work, we investigate the LIBS analysis of gold ore samples of practical interest, namely rock powders and drill cores, and address some of the challenges related to the LIBS analysis for gold ore samples.

To establish the calibration curves (gold signal vs. gold concentration), we used 44 compressed-powder ore samples whose gold concentrations ranged between 0 and 1000 ppm. We first classified the samples using the chemometric principal component analysis (PCA) according to their mineralogical matrix. Different normalization schemes for the gold signal were used to reduce the matrix effects in the calibration curves. These calibration curves were then used to determine the gold concentration of two uncompressed rock powders with different grain sizes (fine- versus medium-grained). We finally performed 2D scans of drill cores from a local mine in Quebec, Canada, and provided an estimation of the averaged gold concentration of these drill cores.

2. Experimental

The experimental setup is schematically shown in Fig. 1. It is mainly composed of 3 components: a laser, a spectrometer and a detector.

2.1 Laser

A Nd:YAG laser (Continuum Surelite I) was used to produce a plasma. This laser can deliver pulse energies of up to 600 mJ at a repetition rate of 10 Hz. The full width at half maximum (FWHM) of the temporal laser pulse profile is 8 ns and its fundamental wavelength is 1064 nm. The beam profile has a Gaussian transverse shape and its divergence is 0.8 mrad (full angle).

2.2 Spectrometers

a. McPherson spectrometer

We used a Czerny-Turner spectrometer (McPherson model 207) with a focal length of 0.67 m and a numerical aperture of F/5.8. The spectrometer was equipped with a grating of 2400 lines/mm blazed at 300 nm. This grating can cover wavelengths ranging from 180 nm to 650 nm. The corresponding reciprocal linear dispersion is about 0.53 nm/mm at 267 nm. Rotation of the grating was controlled by a stepper motor. The bandpass of this spectrometer is 15.5 pm at 267 nm, with equal input and output slit widths of 25 μm.

b. Avantes spectrometer

We also used a small compact spectrometer with Czerny-Turner configuration, but with a resolution lower than the McPherson spectrometer. It offers a wide range of wavelengths from 190 nm to 750 nm. The purpose of this spectrometer is to provide more information on the laser induced plasma for characterisation purposes and enable to achieve adequate normalization of the intensity of the gold line for a given gold bearing matrix.

2.3 Detector

An intensified charged-coupled device (ICCD) camera (Istar DH720-25H-05, Andor Technology), coupled to the McPherson spectrometer described above, completed the detection system. This camera contains 1024x256 pixels on the photosensitive surface. The dimensions of each pixel are 26x26 μm^2. Therefore, the pixel resolution with the McPherson spectrometer is 12 pm/pixel at 267 nm which allows a spectral measurement window of 12.3 nm.

The laser beam was focused onto the surface of the samples by a 20-cm focal length lens to generate a plasma. The samples were mounted on a triple axis motorized stage (Newport, UTM 100 mm) driven by a programmable controller (Newport, model ESP 300). The plasma emission was reflected on the dichroic mirror and then divided into two parts by means of a window, so that 8 % of the light was focused by a corrected triplet into an optical fiber connected to the Avantes spectrometer. The remaining 92 % of the emitted light was also focused by a corrected triplet into the circular input end of an optical fiber bundle composed of twenty five 100-μm diameter fibers. The vertically aligned output of this bundle was positioned in front of the entrance slit of the McPherson spectrometer to match the ICCD array and maximise the signal-to-noise ratio.

2.4 Samples

In ore samples, gold can be found in many mineralogical matrix types, such as quartz, pyrite, chalcopyrite, arsenopyrite, dolomite, etc. Within these matrices, gold often appears as native grains (sometimes mixed with silver). In the Canadian mines, gold grain sizes range typically between 0.1 and 100 μm (see Fig. 2.). [14]

In this study we tried to cover a wide range of mineralogical matrices using 44 synthetic matrices made of compressed fine powders with a quasi-uniform concentration of gold. Table 1 provides a list of the samples used in this study with their gold, silicon, sulfur and iron concentration. Most of these samples were obtained commercially, along with the analysis of their elemental composition.

As we will see later in this study (section 3.5), due to the discrete nature of gold distribution in mining samples (rock or drill-core) the concentration of gold can reach the % level within the area enclosed by the laser spot. This concentration can drop to zero in another area. In order to extend the calibration curves toward such high concentrations, high gold concentration samples of compressed powder had to be prepared in our laboratory since such samples are hardly available commercially. For preparing those samples, we used gold solutions to dope the two powder matrices JG-3 (2.58% of iron) and WMS-1 (50.35% of iron). We prepared 6 samples for each of the two matrices with average gold concentrations of: 0.28, 23, 40, 92, 175, 421 and 891 ppm for WMS-1, and 0, 24, 47, 85, 187, 458 and 932 ppm for JG-3. For each sample, we mixed uniformly the gold solution with the powder. We then dried the mixture at a temperature of 60 °C for 24 hours. Then we added 4% polyethylene to each sample to improve cohesion and mixed each sample by a quadratic mixer for 30 minutes. Finally, we compressed the samples using an automatic press at a pressure of 30 tons. The actual average gold concentration in those samples, which are reported above and in Table 1, was determined using instrumental neutron activation analysis.

2.5 Working parameters

In this study, we maintained the energy of the laser at 60 mJ while the diameter of the laser spot was 600 μm. All the measurements were performed at atmospheric pressure.

In the literature, we can find spectroscopic data for a few hundreds of gold lines [15]. Although the energy levels and statistical weights are well documented for the emitter levels of the lines, their transition probabilities and their oscillator strengths are mostly unknown except for the 4 most intense Au I lines: 242.795 nm, 267.59 nm, 312.278 nm and 627.83 nm. The last two lines are weaker than the first two ones. The 242.795 nm and 267.59 nm lines are both resonant lines (linked to the ground state), which means that they may suffer from self-absorption for high gold concentration values. According to the atomic physic data such transition probabilities, statistical weight, energy levels etc. the 242.795 nm appears to be the strongest for gold detection which supposedly will lead to lower detection limit. However in our experimental conditions, the spectral response of our setup (ICCD/ lenses, spectrometer) is better optimised for 270 nm than 242 nm and the line 267.96 appears stronger than 242.73 nm. Furthermore the 242.73 nm suffers from interference with iron lines. We checked with matrices containing elements which may interfere with the gold line and concluded that the 267.59 nm line was suitable for all gold ore samples used in our conditions. For all these reasons, we opted to select the 267.59 nm line for analytical purposes in our conditions.

The measurements on the reference samples were performed by scanning 8 x 8 mm^2 with a step size of 0.8 mm and averaging over 100 laser shots to compensate for the heterogeneous distribution of gold on the surface. Then we repeated this sequence 5 times at the same location in order to provide the standard deviation associated with the measurements.

As it is very well known the laser-induced plasmas are transient in nature, just after the laser pulse, the plasma is characterized by an intense continuum which decreases quickly as the plasma cools down and is replaced by sharp lines. In this study, we used an integration delay of 2 μs (delay before starting to integrate the signal) and a gate width of 10 μs (integration time of the signal). These two values were selected such as to obtain the nearly optimal signal-to-noise ratio for our setup.

3. Results and discussion

3.1 Classification of the reference samples

In order to identify the parameters causing the main variations in the spectra of our reference samples, we analyzed the 44 samples of Table 1 by means of the PCA, a fundamental multivariate method used in chemometrics. The PCA is based on the determination of the variance of the spectra obtained for each sample. [16] We applied the PCA on the spectra acquired with the Avantes spectrometer, between 200 nm and 750 nm. The PCA was carried out using the software Eigenvector, provided by PLS_Toolbox. We used the Auto-scaling and the Multiplicative Scatter Correction (MSC) options, which attempt to account for scaling and offset effects.

The results of the PCA are shown in Fig. 3 as the 2D projection of the data scores on the plane of the first two principal components. Starting from the left of this figure, we find the WMS-1 samples (blue triangles) which contain 50% of iron,

then the two samples of pyrite, containing 40% of iron (green diamonds), followed by the CCU sample which contains 16% of iron (yellow circle), then the LE sample which contains about 13% of iron (cyan inverted triangle). We can also see in this figure that the quartz chlorite and JG-3 samples are grouped very closely (red and green symbols). Actually, the quartz chlorite and JG-3 samples contain 5% and 2.5% of iron, respectively, which explains their close location in the plane. Thus the first principal component PC1, which represents 83.13% of the variables, indicates that the iron concentration is the leading parameter causing changes in the spectra. The component PC2, which represents 9 % of the variables, does not seem to have a clear meaning. Our 44 reference samples thus fall into two categories: the Fe-rich samples containing 13% of iron or more and the Si-rich samples containing 5% of iron or less.

3.2 LIBS spectra of compressed powder samples (reference materials)

Figure 4 shows 2 spectra between 265 and 270 nm obtained from 2 different mineralogical composition samples. The blue and green curves (lower and higher intensity, respectively) were obtained from a quartz chlorite (Si-rich) and a pyrite (Fe-rich) sample, respectively. The quartz chlorite sample (QC7 in Table 1) contains 31 ppm of gold and 4.99% of iron while the pyrite sample (PYRITE2 in Table 1) contains 25.4 ppm of gold and 39.55% of iron. As expected from the PCA, we observe significant changes in the spectra as the iron concentration increases.

On the spectrum of the quartz chlorite sample, we identified the gold line at 267.59 nm and the ionic chromium line at 267.71 nm. The highest peaks of this spectrum correspond to aluminum and iron lines. As we can see, the gold line is well resolved on this spectrum. However, for the Fe-rich matrix, two iron lines appear next to the gold line, which causes a significant offset when extracting the net intensity of the gold line. In order to evaluate this offset, one needs to determine the signal for the blank sample (without gold) at the position of the gold line (267.59 nm). For example, we found an offset of 50 counts in the case of the quartz chlorite sample, while an offset of 500 counts was measured in the case of the pyrite sample, using QC1 (0.08 ppm of Au, 5% of Fe) and WMS-1 (0.279 ppm of Au, 50.4% of Fe) as blank samples, respectively. This offset depends mainly on the iron concentration. We note that evaluating the offset in a real sample such as a drill-core or a rock is also relatively easy because blank samples are readily available at gold-free spots on the sample surface.

3.3 Calibration curve

When establishing the calibration curve (gold concentration vs. gold signal intensity) using 36 of our reference samples (8 Si-rich samples used for validation were not included in the calibration set), one finds two distinct curves, as shown in Fig. 5: one for the Si-rich samples ([Fe] ≤ 5%) and one for the Fe-rich samples ([Fe] > 13%). In the calibration curves of Fig. 5, the gold intensity (I) at 267.59 nm has been normalized by the integral of the whole spectrum (I_0) obtained by the

Avantes spectrometer between 200 nm and 750 nm. For both curves the intensity ratio I/I_0 shows good linearity with the gold concentration up to about 200 ppm and then starts leveling, likely due to the self-absorption of the gold line. Since the 267.59 nm gold line is a resonant line, the self-absorption probability increases with the gold concentration, as is well documented in the LIBS literature [17]. The red and purple solid lines represent quadratic fits for the Si-rich and Fe-rich samples, respectively, with a good coefficient of determination R^2=0.99497 and 0.99796, respectively. The relative standard deviation (RSD) of the 5 replicas of 100 shots each is about 2-5%, as shown by the error bars.

Based on the usual criterion that the minimum detectable intensity of the gold line is three times the level of the background noise [18] and taking into account the slope obtained by the calibration curve, the limit of detection (LOD) for gold is estimated to be 0.75 ppm for the Si-rich samples and about 1.5 ppm for the Fe-rich samples.

We have also established calibration curves using the net intensity of the gold line normalized to the adjacent background at 267.38 nm (see Fig.4). This position is always free of interfering lines, regardless the mineralogical matrix. For the latter normalization, the coefficient of determination and the RSD are quite similar to those obtained by normalizing with respect to the whole spectrum I_0 and the LOD was 0.74 ppm for Si-rich samples. However, when using the net intensity (without normalization), the coefficient of determination was not as good (R^2=0.9012), the

RSD was about 10-15 % and the LOD was 0.87 ppm for the Si-rich samples. The same trends were observed in the case of Fe-rich samples.

We validated the calibration curve for the Si-rich samples shown in Fig. 5 by predicting the gold concentrations for 8 Si-rich samples that were not taken into account when establishing the calibration curve. For this purpose, we determined the gold concentration corresponding to the measured intensity ratio I/I_0 using the equation obtained from the quadratic regression over data points $C = 5.49\text{x}10^6(I/I_0)^2 + 71814(I/I_0) + 0.14$, where C is the gold concentration. Note that the corresponding quadratic regression for the Fe-rich curve was $C = 4.24 \text{ x } 10^7(I/I_0)^2 + 48110(I/I_0) + 3.96$. These two equations will be used for the prediction of the gold concentration in the drill-cores, as we will see in section 3.5.

Figure 6 shows the predicted gold concentrations as a function of the laboratory assay of gold concentration for the 8 validation samples. The dashed line represents a linear curve with a slope of 1 while the solid line is the linear regression over the 8 concentrations. As we can see on this figure, the predicted concentrations fit well the actual concentrations obtained by the laboratory assay with $R^2 = 0.9973$ and an average relative error of 15.8%. Table 2 shows the laboratory assay values and the LIBS measurements of the gold concentrations along with the relative error of the LIBS measurement. The estimated error on the LIBS measurements was obtained from the RSD. Unfortunately, the number of Fe-rich samples was not large enough to keep some of them for validation.

3.4 Gold concentration in uncompressed powders

As a first assessment of the influence of heterogeneity on LIBS concentration measurements for mining samples of practical interest, we have analysed two types of uncompressed powders provided by Barrick Gold Corporation (Canada): fine and medium-grained powders with known gold concentrations of 5.4 ppm and 12.4 ppm, respectively. As shown in Fig. 7, the average grain size is smaller than a millimeter for the fine powder while it is a few millimeters for the granular powder. . The fine powder was a mix of quartz (31%), calcite (36 %), dolomite (9%), muscovite (7%) and pyrite (2%), whereas the granular powder was a mix of quartz (38 %), calcite (40 %), dolomite (19 %) and muscovite (2.5 %). Therefore, these two samples belong to the Si-rich category.

We put about 10 g of powder in a cylindrical container with a diameter of about 5 cm (Figure 7) and then performed 500 laser shots at different locations on the surface. The laser spot size was about 600 μm while the distance between the shots was 800 μm. The gold concentration was determined from LIBS measurements using an averaged spectrum of 500 shots. The RSD was obtained from 5 replicas of 100 shots each. A RSD value of about 2-5%, similar to that of compressed powder, was obtained for the fine powder and a RSD value of about 5-10% was obtained for the granular one. This difference could be attributed to the more uniform distribution of gold in the fine powder as compared to the granular powder, whose grains are larger on average than the laser spot (few mm vs. 600 μm). Table 3 shows the gold concentration of these powders obtained using the

calibration curves for the Si-rich samples of Fig. 5 (normalized with respect to I_0) and also using the calibration curves obtained without normalization and with normalization with respect to the background. The relative error with respect to the actual gold concentration is also given. The LIBS measurement of the gold concentration is more accurate for the fine powder than for the granular powder for the three normalization schemes used. Table 3 also shows that the best prediction was achieved when normalizing by the adjacent background for both samples. Note that T. Stehrer *et al.* [19] have observed similar values of temperature and electron density in Fe_2O_3 for compressed and uncompressed powders. This result suggests that the calibration curve established using compressed fine powders can be used to predict the concentration of uncompressed ones. However, this equivalence might not hold for the granular powder which is made of solid chunks on the scale of the laser spot. Plasmas produced from compressed powders and solids could have different properties. This may explain why the LIBS concentrations for the granular powder are systematically higher than the reference values. More samples should be analyzed to confirm this trend.

3.5 Mapping and average gold concentration on the surface of a drill core

We analyzed three drill cores from the Lapa gold mine (Québec, Canada). The cores were solid cylinders of about 1 meter long and 7 cm diameter (Figure 8). The cores have been cut lengthwise into two parts. One half has been grinded and homogenised, and then analysed by fire assay. The averaged concentrations

reported on each 1 meter long cores were 46 ppm, 21 ppm and 10 ppm, respectively. We have performed 10 000 laser shots onto the flat surface of the other half of the core with a laser-scanned area of 5x20 cm^2. The laser spot size was about 600 μm while the distance between the shots was 800 μm. We have then determined the gold concentration for each laser shot on the surface using the quadratic fits $C(I/I_0)$ of the calibration curves shown in Fig. 5. Figure 9 shows the 3D mapping of the gold concentration over the 5x20 cm^2 area for the core whose other half contains 46 ppm of gold. As one can see in Fig. 9, gold concentrations were locally high (up to few thousands ppm) and very low for other positions, highlighting the heterogeneous distribution of gold in the rock matrix over a millimeter scale. This result is consistent with the discrete distribution of gold in the rock matrix discussed previously (Fig. 2). Note that although the highest gold concentration used in our calibration curves was 1000 ppm, we were able to determine higher concentrations by extrapolating the two polynomial fits $C(I/I_0)$ for the Si-rich and Fe-rich cases.

Figure 10 shows the concentration of gold averaged over an area of 5x1 cm^2 as a function of the position along the core axis. As can be seen, the concentration of gold also changes significantly over the centimeter scale. Table 4 shows the predicted averaged concentration for the 3 cores and their relative standard deviations (RSD) taken over the 20 areas of 5x1 cm^2. As we can see the RSD values vary from 55% to 92%, highlighting again the strong heterogeneity of gold in the cores.

As seen in Table 4, averaging the gold concentration over the 10 000 laser shots resulted in values of 23.5 ppm, 11.1 ppm and 5.6 ppm, respectively. To evaluate the gold concentration, we used the intensity of the continuum at 267.36 nm: when this intensity was smaller than 1 000 counts, we used the Si-rich calibration curve of Fig. 5; otherwise we used the Fe-rich calibration curve. Although we have not measured the concentration of iron in our cores, we are sure that it is lower than 50% (the iron concentration of the WS1 samples used for establishing the calibration curve). The gold concentration values obtained are systematically about two times lower than the fire assay reference values, which means an error of about 50% in the 3 cases. Note that this trend is opposite to that of the granular powder of the previous section, where the concentrations were systematically higher than the reference values.

4. Conclusion

In summary, in this work we have used LIBS for evaluating the concentration of gold in mineral samples of practical interest, namely fine and granular powders and drill cores. The calibration curve was established using 44 synthetic samples made of compressed powders of different compositions containing a quasi-uniform distribution of gold. The PCA analysis of our samples revealed that the iron concentration accounts for about 83% of the variance of our spectra. Consistently, the calibration curve for the Au I 267.59 nm line splits into two branches: one for Si-rich samples (< 5% iron) and one for Fe-rich samples (> 13% iron) with limits of detection of 0.8 ppm and 1.5 ppm, respectively, thus nearly fulfilling the needs of

the mining industry in term of the detection limit for the measure of gold concentration (~1 ppm). We showed that normalizing the gold line intensity with respect to the integrated spectrum intensity or with respect to the spectral background close to the gold line improves the regression fit of the calibration curves, as compared to not normalizing. The use of one branch or the other of the calibration curve can be determined from the number and intensity of the iron lines of the spectra.

The application of this calibration curve to the case of uncompressed mineral powders showed that gold concentrations closer to the reference values are obtained for the fine powder as compared to the granular powder. Consistently, a RSD of 2-5% was obtained for the fine powder and about twice as much for the granular powder. In addition, we found that normalizing with respect to the spectral background provided the most accurate results in those cases. For the granular powder, the LIBS measurements using the 3 normalizations of the gold line intensity were systematically higher than the reference values by at least 46%.

A 10 000 laser shot LIBS analysis has also been performed on a 5x20 cm^2 area of the flat surfaces of 3 half cores cut lengthwise. The 2D scan of the gold concentration obtained shows the multiscale heterogeneous distribution of gold on the surface. The concentrations obtained are about two times lower than the reference values determined by fire assay from the full 1-meter other half of the core. Several reasons can explain this result. A first possible reason is the strongly heterogeneous nature of the gold distribution on the core surface, even on the centimeter scale, so that the relatively small 5x20 cm^2 scanned area is not

representative of the whole core. Other possible reasons include the calibration curves established for compressed powders, and the possibility that the surface concentration may not reflect accurately the volume concentration of the cores. This could happen for example if the lengthwise cutting process would induce surface alterations of the cores, such as removal of part of the gold grains. One notes that for the fine powder the surface is more representative of the bulk and the agreement within the uncertainty of the measurement seems better than for the core and granular samples.

The present work constitutes a first step toward determining the gold concentration in practical mineral samples using LIBS. As pointed out above, several questions remain to be addressed. In the light of the investigation presented in this paper, the main questions are the following. (1) Does the calibration curve established from compressed powders can be used for solid samples such as granular powder or rocks? (2) Does the cutting process of drill cores or rocks affect the gold concentration at the surface of the sample? (3) How to automatically identify the gold concentration independently of the matrix? (4) How to scan the rock samples in an optimal way, i.e. how to minimize the effects of heterogeneity of the gold concentration with a minimal number of laser shots? All these questions are currently under investigation.

References

[1] R. H. Sillitoe (2010) The challenge of finding new mineral resources: an introduction. Society of Economic Geologists, Special Publication 15, p. 1.
[2] Mining Association of Canada (2012), F&F 2012: Facts and Figures of the Canadian Mining Industry and R. Meyers, VP Technical Affairs, Mining Association of Canada, presentation to Canada Mining Innovation Council, Jan 2012 and F. Robert, Presentation to CMIC Signature Event, Toronto Feb 2013.
[3] G.E. De Benedetto et al, Infrared spectroscopy in the mineralogical characterization of ancient pottery, Journal of Cultural Heritage 3 (2002) 177–186
[4] Canadian mining industry research organization (CAMIRO) exploration division: Quality Control Assessment of Portable XRF Analyzers: Development of Standard Operating Procedures, Performance on Variable Media and Recommended Uses, CAMIRO project 10E01, Phase I, June 9, 2011.
[5] D. A. Cremers, L. J. Radziemski, Handbook of Laser-Induced Breakdown Spectroscopy. J. Wiley (2013), p. 437.
[6] K.J. Grant, G.L. Paul, J.A. O'Neill, Quantitative elemental analysis of iron-ore by Laser-induced Breakdown Spectroscopy, Appl. Spectrosc. 45 (1991) 701–705.
[7] K.J. Grant, G.L. Paul, J.A. O'Neill, Time-resolved Laser-induced Breakdown Spectroscopy of iron-ore, Appl. Spectrosc. 44 (1990) 1711–1714.
[8] Q. Sun, M. Tran, B.W. Smith, J.D. Winefordner, Determination of Mn a nd Si in iron ore by Laser-induced Plasma Spectroscopy, Anal. Chim. Acta 413 (2000) 187–195.
[9] D. Michaud, R. Leclerc, Proulx, Influence of particle size and mineral phase in the analysis of iron ore slurries by Laser-induced Breakdown Spectroscopy, Spectrochim. Acta Part B 62 (2007) 1575–1581.
[10] D. Michaud, E. Proulx, J.-G. Chartrand, L. Barrette, Shooting slurries with Laser-induced Breakdown Spectroscopy: sampling is the name of the game, Appl. Opt. 42 (2003) 6179–6183.
[11] J.A. Bolger, Semi-quantitative Laser-induced Breakdown Spectroscopy for analysis of mineral drill core, Appl. Spectrosc. 54 (2000) 181–189.
[12] D. I. Death, A. P. Cunningham et L. J. Pollard, Multi-element analysis of iron pellets by laser-induced breakdown spectroscopy and principal components regression, Spectrochim. Acta Part B 63 (2008) 763-769.
[13] M. Dalm et M. Buxton, Characterizing theeconomic value of an epithermal Au-Ag ore with Laser Induced Breakdown Spectroscopy (LIBS): possibilities and limitations. Conference paper, February 2016
[14] D. C. Harris, the mineralogy of gold and its relevance to gold recoveries, Geological survey of Canada contribution Number 13089, July 3, 1990.
[15] NIST Atomic Spectra Database Lines Data.
[16] Jackson, J.E., 1991. A User's Guide to Principal Component Analysis.
John Wiley and Sons, New-York, USA.
[17] M. Sabsabi, P. MCielo, Quantitative analysis of aluminum alloys by Laser-induced breakdown spectroscopy and plasma characterization, Appl. Spectros. 1995, 49 (4) 499-507
[18] UPAC, General Aspects of Trace Analytical Methods-IV. Recommendations for Nomenclature, Standard Procedures and Reporting of Experimental Data for Surface Analysis Techniques, 1979, vol. 51, p. 2247.
[19] T. Stehrer, B. Praher, R. Viskup et al, Laser-induced breakdown spectroscopy of iron oxide powder, J. Anal. At. Spectrom., 2009, 24, 973–978 | 973

Figures

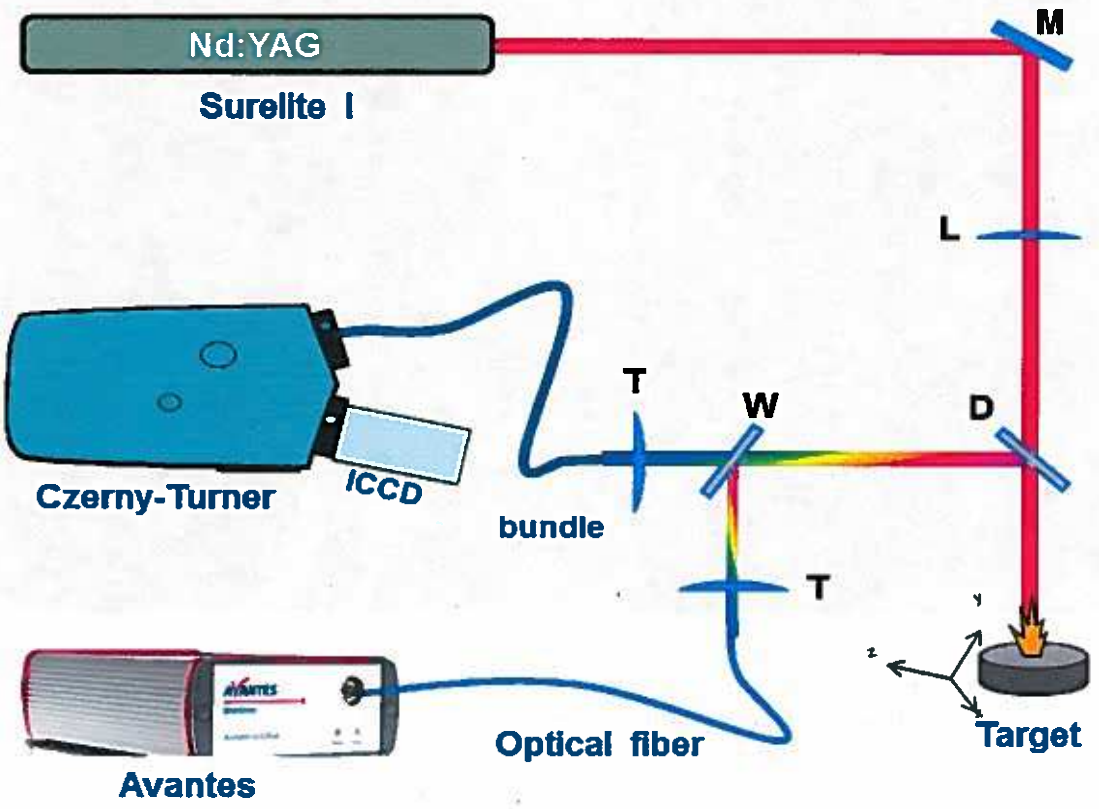

Fig.1. Schematic representation of the experimental set-up.

Fig.2. Spatial distribution of the gold grains (brightest spots) on a drill core from the Lapa mine (Québec, Canada) obtained using a scanning electron microscope.

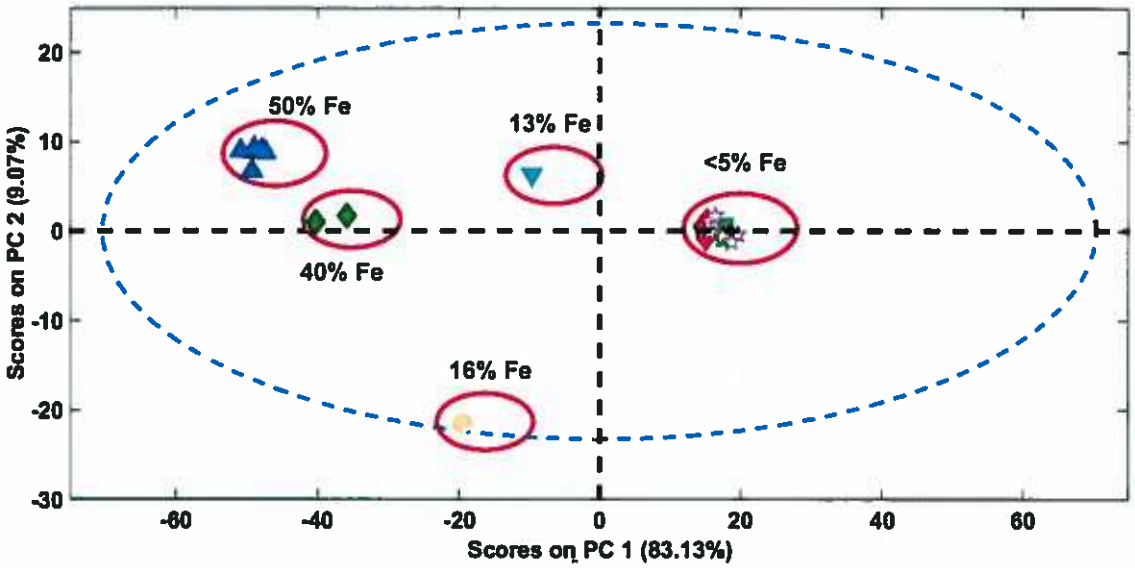

Fig.3. PCA scores plot for the samples presented in Table 1.

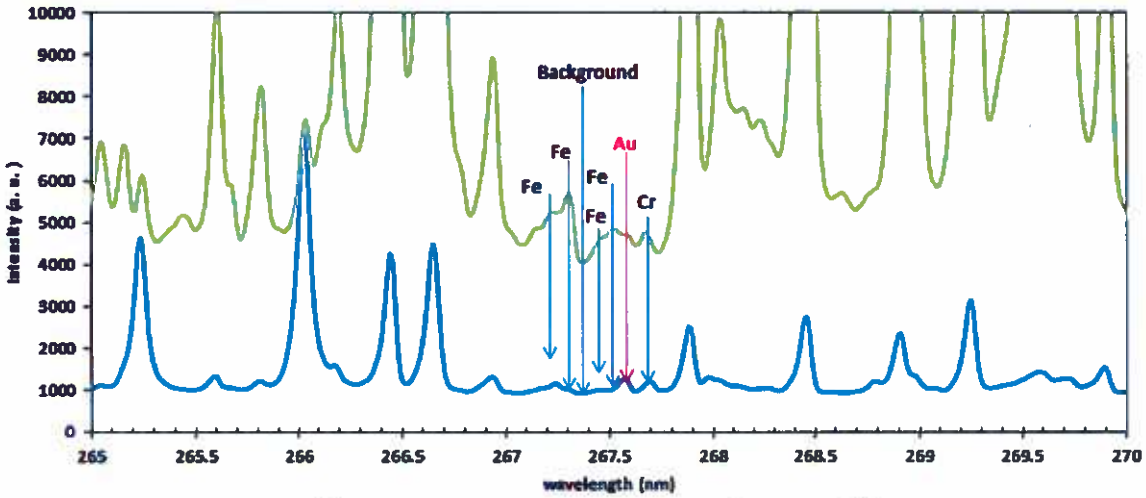

Fig.4. Spectra between 265 and 270 nm for two different mineralogical matrices. Blue: QC7 (31 ppm of Au, 5% of Fe); green: PYRITE2 (25 ppm of Au, 39.6% of Fe) as shown in Table 1

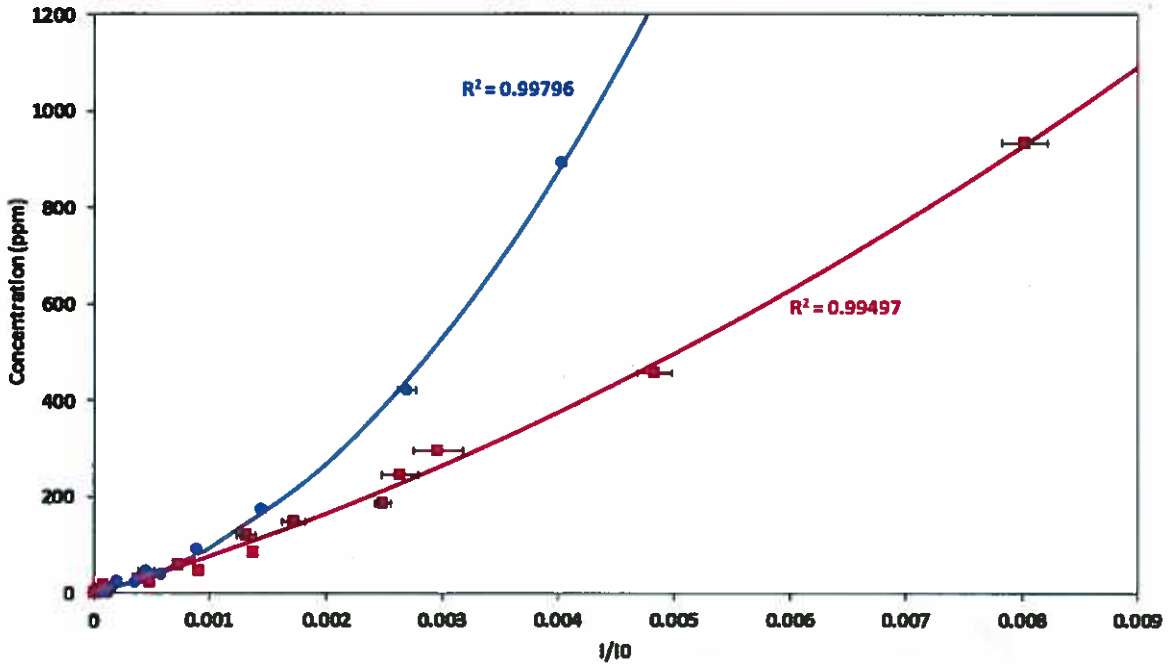

Fig.5. Calibration curves (Concentration vs I/I_0) using the gold line at 267.59 nm for the silicon-rich samples (squares) and for the iron-rich samples (circles). The two solid lines represent the quadratic regression fit of the points from each sample set.

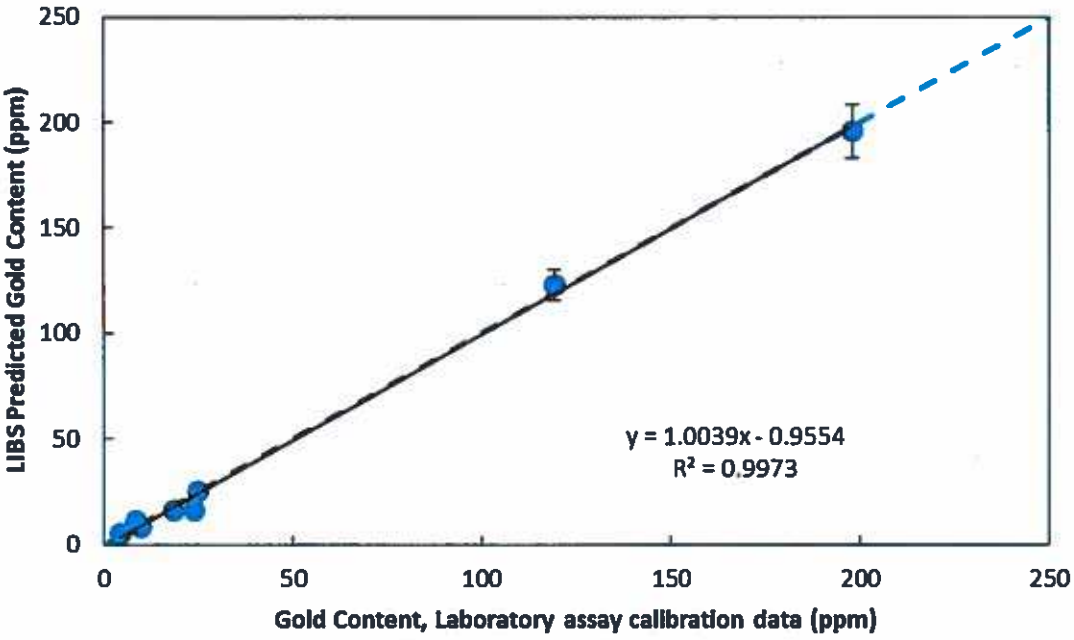

Fig. 6: A plot showing the predicted gold concentrations as a function of laboratory assay gold concentrations. The dashed line is the unity slope while the solid line represents the linear regression of these points.

Fig.7: Picture of the two types of powder involved in this study, showing the quantity used for the analysis. The left container is filled with the fine powder and the right one with the granular powder.

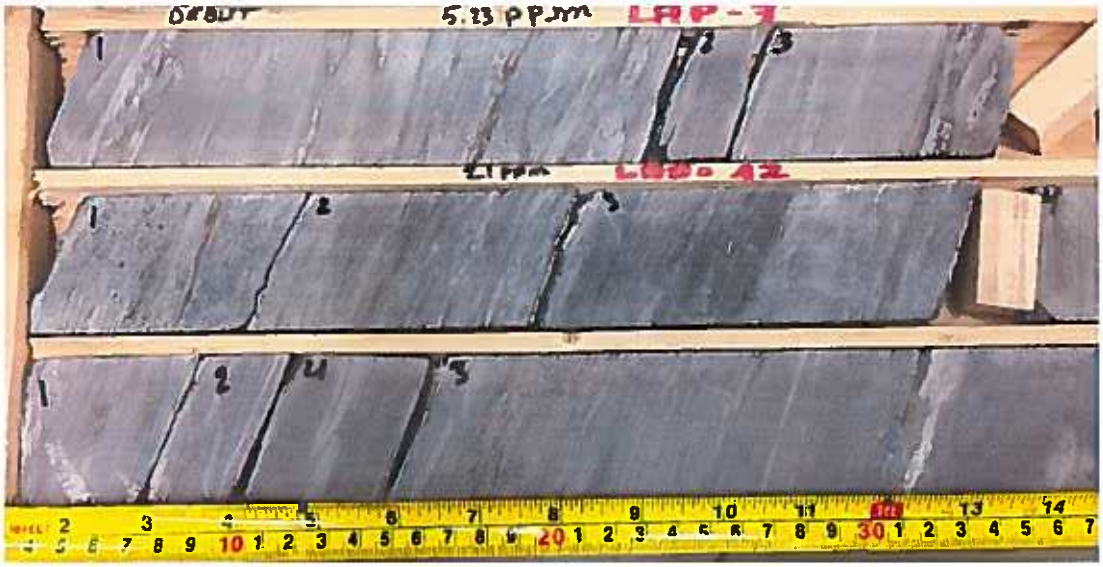

Fig.8. Parts of 3 cylindrical drill cores cut lengthwise.

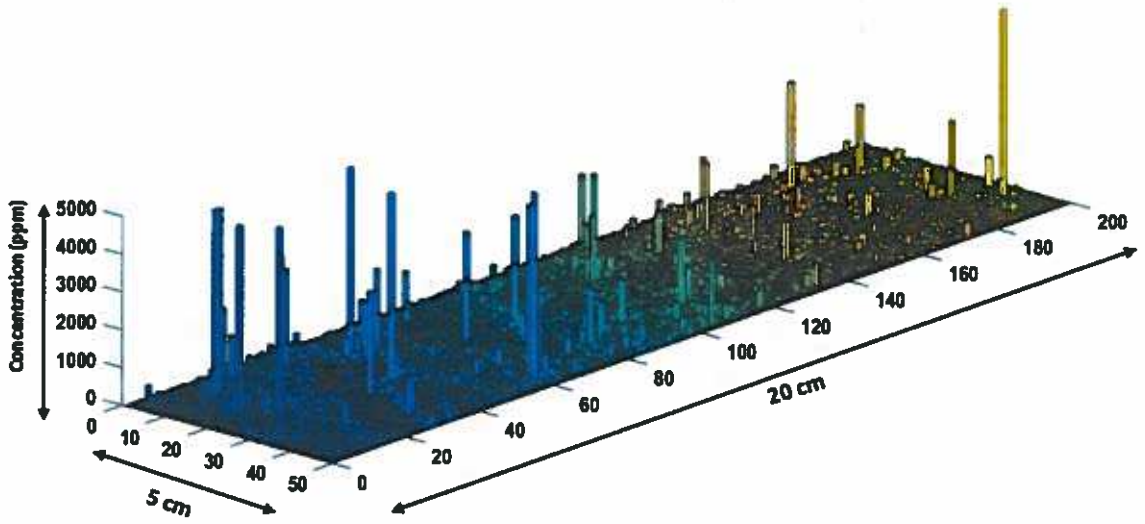

Fig.9. 3D mapping of an area of 5 x 20 cm^2 of a drill core from the Lapa mine. The averaged gold concentration over the entire drill core is 46 ppm.

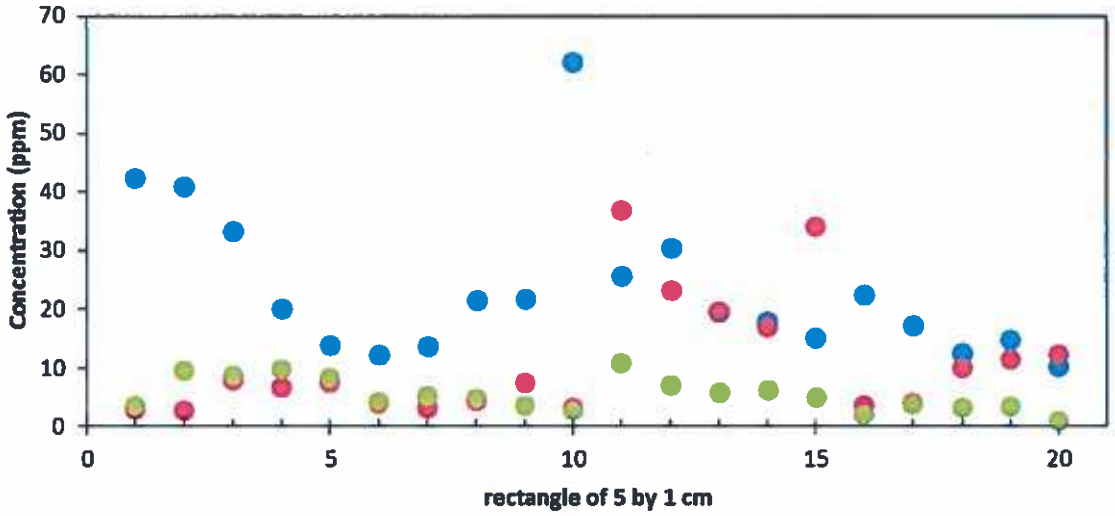

Fig. 10. Gold concentration as a function of different areas of 5 cm x1 cm for three drill cores, namely 46 ppm (blue circles), 21 ppm (red circles) and 10 ppm (green circles)

Table captions

	Identification	Type	Producer	[Au] ppm	[Si] %	[S] %	[Fe] %
1	QC1	Quartz-Chlorite	COREM	0.08	16.9009	0.8476	4.9872
2	QC2	Quartz-Chlorite	COREM	0.8	16.9009	0.8476	4.9872
3	QC3	Quartz-Chlorite	COREM	4	16.9009	0.8476	4.9872
4	QC4	Quartz-Chlorite	COREM	5.2	16.9009	0.8476	4.9872
5	QC5	Quartz-Chlorite	COREM	7	16.9009	0.8476	4.9872
6	QC6	Quartz-Chlorite	COREM	11.8	16.9009	0.8476	4.9872
7	QC7	Quartz-Chlorite	COREM	31	16.9009	0.8476	4.9872
8	QC8	Quartz-Chlorite	COREM	58	16.9009	0.8476	4.9872
9	QC9	Quartz-Chlorite	COREM	119	16.9009	0.8476	4.9872
10	QC10	Quartz-Chlorite	COREM	148	16.9009	0.8476	4.9872
11	QC11	Quartz-Chlorite	COREM	198	16.9009	0.8476	4.9872
12	QC12	Quartz-Chlorite	COREM	247	16.9009	0.8476	4.9872
13	QC13	Quartz-Chlorite	COREM	296	16.9009	0.8476	4.9872
14	QC14	Quartz-Chlorite	COREM	296	16.9009	0.8476	4.9872
15	CCU1		COREM	2.8	16.0930	12.7300	16.4481
16	CCU2		COREM	5.6	16.0930	12.7300	16.4481
17	MA1		COREM	4	24.7674	1.2110	5.0157
18	MA2		COREM	7.1	24.7674	1.2110	5.0157
19	MA3		COREM	10	24.7674	1.2110	5.0157
20	MA3		COREM	20	24.7674	1.2110	5.0157
21	PYRITE1		COREM	10.7	12.9947	21.4879	39.5481
22	PYRITE2		COREM	25.4	12.9947	21.4879	39.5481
23	WMS-1	PGE sulf	CANMET	0.279	2.1500	33.0000	50.3600
24	WMS-1	PGE sulf	CANMET	23	2.1500	33.0000	50.3600
25	WMS-1	PGE sulf	CANMET	40	2.1500	33.0000	50.3600
26	WMS-1	PGE sulf	CANMET	92	2.1500	33.0000	50.3600
27	WMS-1	PGE sulf	CANMET	175	2.1500	33.0000	50.3600
28	WMS-1	PGE sulf	CANMET	421	2.1500	33.0000	50.3600
29	WMS-1	PGE sulf	CANMET	891	2.1500	33.0000	50.3600
30	JG-3	Granodiorite	GSJ	0.00017	31.4400	0.0060	2.5810
31	JG-3	Granodiorite	GSJ	24	31.4400	0.0060	2.5810
32	JG-3	Granodiorite	GSJ	47	31.4400	0.0060	2.5810
33	JG-3	Granodiorite	GSJ	85	31.4400	0.0060	2.5810
34	JG-3	Granodiorite	GSJ	187	31.4400	0.0060	2.5810
35	JG-3	Granodiorite	GSJ	458	31.4400	0.0060	2.5810
36	JG-3	Granodiorite	GSJ	932	31.4400	0.0060	2.5810
37	5#3		COREM	4.2			
38	10#2		COREM	8.27			
39	20#-1-		COREM	18.7			
40	AURM 1		COREM	9.6			
41	AURM 2			23.9			
42	200X2/3#20		COREM	120			
43	SRM 610		NIST	25	33.6000		0.0458
44	MASS	Polymetal sulfide	USGS	47		27.6000	15.6000

Table1: Samples used in this study with their elemental composition.

Lab assay gold concentration (ppm)	Gold concentration measured with LIBS (ppm)	Relative error on measured concentration (%)
4.2	4.9 ± 2.98	17.7
8.27	11 ± 2.04	33.1
9.6	8.3 ± 1.06	13.8
18.7	16.2 ± 4.36	13.1
23.9	15.9 ± 3.22	33.4
25	25.4 ± 1.38	1.8
119	122.9 ± 7.27	3.3
198	195.8 ± 12.59	1.1

Table 2: Laboratory assay and gold concentrations measured with LIBS

Samples	Net intensity	Relative error (%)	I/Continuum	Relative error (%)	I/I_0	Relative error (%)
Fine (5.45 ppm)	3.4	**38**	5.5	**1**	6.8	**25**
Granular (12.37 ppm)	18.8	**52**	18.1	**46**	22.6	**83**

Table 3: Measured gold concentrations and associated errors on two types of uncompressed powder using different normalizations for the gold line.

	Measured average concentration (ppm)	Relative standard deviation (%)
DC1 (46 ppm)	23.32	55.3
DC2 (21 ppm)	11.1	91.6
DC3 (10 ppm)	5.8	62.2

Table 4: Measured average concentrations for the 3 drill-cores (DC) and relative standard deviation as determined from the 20 longitudinal positions.